AIAA Propulsion and Energy Forum
July 9-11, 2018, Cincinnati, Ohio
2018 Joint Propulsion Conference

10.2514/6.2018-4965

Analysis of detonation structures with hydrocarbon fuels for application towards rotating detonation engines

Takuma Sato*
University of Michigan, Ann Arbor, MI, 48109, U.S.A

Venkat Raman†
University of Michigan, Ann Arbor, MI, 48109, U.S.A

Rotating Detonation Engines (RDEs) provide a promising approach to increasing efficiency of gas turbine combustors by utilizing detonation-driven combustion process. While RDEs have been studied extensively in the past, much of this work has focused on the use of hydrogen as fuel. In order to develop RDEs for power generation applications, it is necessary to understand the physics of hydrocarbon detonation. This study utilizes detailed chemical kinetics to simulate a sequence of hydrocarbon-based canonical RDE configurations. The cases emulate ethylene and methane detonation in air with varying degrees of hydrogen dilution as well as a range of operating conditions. The results indicate the while ethylene-based detonations are not significantly affected by the addition of hydrogen, methane mixtures exhibit large changes to the detonation structure. In particular, the critical pressure at which heat release reaches a peak changes to lower values as the hydrogen concentration in the reactant mixture is increased. Detailed comparisons with one-dimensional profiles and the impact of back pressure on the detonation and post-detonation flow are analyzed. Further, profiles of species extracted from the simulations are compared with one-dimensional detonation profiles. Comparisons with theoretical models for thrust and specific impulse are also provided. It is established that the use of detailed chemical kinetics provides a reliable approach to assessing the performance characteristics of RDEs.

I. Introduction

Rotating detonation engines are gaining interest as a promising technology for increasing efficiency of gas turbine combustors [1, 2]. RDEs utilize detonations instead of deflagrations to process the fuel-air mixture, which leads to a gain in pressure accompanying the chemical reactions. Although technology concepts using continuous detonations for energy conversion has existed for many decades [3, 4], there has been a recent surge in interest due to advances in combustor materials and fundamental understanding of the physics of such detonation processes. Of particular interest here is the use of RDEs in natural gas based power generation. While there are numerous RDE studies focused on the use of hydrogen as fuel [1, 5–15], relatively few works have studied other fuels including ethylene [16, 17], propane and other higher hydrocarbons [18], or NO-enhanced hydrogen mixtures [19]. Methane-based detonation processes have been studied in the context of rocket combustors, where methane/oxygen mixtures have been used [20]. However, for stationary power generation, the oxidizer will be compressed air. It is well known that the detonability of methane/air mixtures are very low [21], but these conclusions are based on ambient conditions for the fuel-air mixture. Since stationary gas turbines operate at pressure, the impact of compressed air on the detonation characteristics needs to be studied.

Due to the inherently harsh environment inside an RDE, experimental techniques to probe the detonation structures are severely limited. Although numerical techniques are useful, the complexity of practical RDEs reduce their tractability, especially for complex fuels. As a compromise, canonical flow configurations that represent the essential features of the RDE are typically studied. A linear channel [22, 23] is often use experimentally to capture the macroscopic features of the detonation process. This linear channel consists of a set of injectors issuing into a confined channel from the bottom wall. A detonation wave is then introduced from a transverse boundary that sweeps through the domain. Typically, a single wave or a few temporally-spaced waves are studied [22]. From a computational standpoint, a periodic analog of the linear channel is the unwrapped RDE [6, 24], which assumes that the two end of the linear channel are periodic.

*Graduate Student, Aerospace Engineering Department, takusato@umich.edu
†Professor, Aerospace Engineering Department, ramanv@umich.edu

Since the detonation channel is thin compared to the length of the combustor, the flow is assumed to be two-dimensional, which vastly reduces the computational expense. While such canonical flows use premixed fuel-air mixtures, practical RDE configurations are based on non-premixed injection with turbulence-driven mixing inside the combustor prior to chemical reactions. Nevertheless, the canonical flows have been useful in elucidating the detonation processes. In order to increase the relevance of these studies to practical geometries, different injection boundary conditions have been used [25–27]. For instance, the injection plane is divided into discrete sections to emulate the finite set of injectors in a practical system [27].

In simulating detonating flows, another equally important consideration is the choice of chemical kinetic mechanism. Although reaction mechanisms are available for many different fuels, these are typically developed for deflagration processes, and their accuracy in capturing detonations has not been fully evaluated [28, 29]. Further, detailed mechanisms can be computationally expensive due to the large numbers of reactive species involved. In some studies, models for detonation based on a one-dimensional representation of detonation processes have been considered [17, 30], while other studies have utilized one-step chemistry [31, 32]. Other studies have considered deflagration-based kinetic mechanisms and have reproduced the basic characteristics of the detonation process [16, 33, 34]. Development of detailed chemical mechanisms is further impeded by the fact that most measurements are not spatially or temporally resolved to obtain details of the inner structure of the detonation wave. As a result, macroscopic measurements such as detonation wave speed or post-detonation conditions are used for calibrating models, which are severely limited (See comment by Radulescu in [29]).

These studies revealed some essential features of hydrocarbon-based detonations. The CJ velocity does not show a conclusive trend in terms of the number of carbon atoms. While hydrogen/air detonation exhibits the highest detonation speed, ethylene and propane both exhibit higher speeds than ethane [18]. Further, the differences in the thrust or specific impulse of the RDE was controlled by the thermodynamic properties of the mixture rather than the fluid dynamics or the reaction structure. In other words, if detonable conditions are reached, the fluid dynamics does not play an important role. However, this conclusion may not be valid near the limits of detonabillity, or when non-premixed injection is used. The wave speed reaches a maximum around an equivalence ratio of $1.2 - 1.5$ for most hydrocarbon mixtures. The height of the detonation wave in linear channels is also found to be a function of equivalence ratio, with the minimum length reached for maximum wave speed [35]. It was found that an equivalence ratio range of $0.8 - 1.3$ yielded successful stabilization of detonations for ethylene-air based RDEs with ambient backpressure conditions [36].

This discussion shows that although there have been number of studies aimed at RDEs, there has been relatively low focus on natural gas based combustion. Further, many of these studies consider high injection to back pressure ratios, leading to supersonic flow near the exit of the RDE and low pre-detonation pressure within the chamber. The focus of this work is to address these gaps in knowledge by conducting two-dimensional detailed chemistry simulations of methane/ethylene/hydrogen mixtures at conditions relevant to stationary gas turbines. The periodic linear channel is chosen as the test system. The impact of operational quantities such as injection pressure, back pressure and injection temperature is studied by analyzing the detailed flow field information.

II. Computational Approach

The computational approach is based on solving the conservation equations for mass, momentum, enthalpy and the species mass fractions. The ideal gas law is used to close the system of equations. The governing equations in conservative form are written as

$$\frac{\partial \rho}{\partial t} + \frac{\partial \rho u_i}{\partial x_i} = 0, \tag{1}$$

$$\frac{\partial \rho u_i}{\partial t} + \frac{\partial \rho u_i u_j}{\partial x_j} = -\frac{\partial p}{\partial x_i} + \frac{\partial \tau_{ij}}{\partial x_j}, \tag{2}$$

$$\frac{\partial \rho E}{\partial t} + \frac{\partial \rho u_j H}{\partial x_j} = \frac{\partial}{\partial x_j} k \frac{\partial T}{\partial x_j} + \frac{\partial \tau_{ij} u_i}{\partial x_j}, \tag{3}$$

and

$$\frac{\partial \rho Y_i}{\partial t} + \frac{\partial \rho u_j Y_i}{\partial x_j} = \frac{\partial}{\partial x_j} \rho D \frac{\partial Y_i}{\partial x_j} + \dot{\omega} M_i, \tag{4}$$

where ρ is the mass density, u, v, w are x, y, and z velocity components, respectively, p is the pressure, E is the total energy, and H is the total enthalpy. The viscous stress τ is obtained as

$$\tau_{ij} = -2/3\mu\frac{\partial u_k}{\partial x_k}\delta_{ij} + \mu(\frac{\partial u_j}{\partial x_i} + \frac{\partial u_i}{\partial x_j}), \tag{5}$$

where μ is the viscosity of the fluid. For each species $i = 1, \ldots, N$, where N is the number of species, Y_i is the mass fraction, $\dot{\omega}_i$ is the molar production rate, and M_i is the molecular mass. Note that each species has its own transport equation.

The governing equations are discretized using a finite-volume approach. All the variables are collocated at the control volume centers, and require reconstruction of values at the cell faces for flux evaluations. An unstructured grid approach is implemented within the OpenFOAM framework [37]. The resulting solver is termed UMdetFOAM [38, 39]. A MUSCL-based HLLC scheme, where MUSCL stands for Monotone Upstream-centred Scheme for Conservation Laws and HLL is detonated by Harten, Lax, and van Leer (C stands for Contact) [40, 41] is used for flux reconstruction. The diffusion terms are discretized using the Kurganov, Noelle and Petrova (KNP) approach [42]. A second-order Runge-Kutta approach is used to advance the solutions in time.

One of the key features of this solver is the ability to handle detailed chemical kinetics. This capability is obtained by coupling the OpenFOAM solver to the open source CANTERA [43] package. The CANTERA package can read in mechanism files and provide all reaction rates and thermochemical properties needed to evaluate enthalpy and energy. In the studies shown below, different fuels are used. The chemistry mechanisms for these cases are as follows: a) For ethylene, the Varattharajan mechanism using 21 species and 38 reactions is used [44]; b) for methane, the Petersen mechanism with 22 species and 34 reactions is used [45]. Both these mechanisms allow use of hydrogen as a species, which will be leveraged to study different levels of hydrogen addition to the fuel-air mixture.

The UMdetFOAM package uses the OpenFOAM domain-decomposition based parallelization using MPI communications. The code has been shown to scale linearly up to 65000 cores with and without GPU acceleration. For the simulations below, a lower processor count is used. Below, a sequence of test cases are first used to establish validity of the numerical approach, and then perform the periodic channel studies.

III. Computational Results

Due to the nature of detonations, it is always necessary to perform some fundamental studies to ensure that grid resolution and other numerical parameters do not adversely affect of the results [46]. Consider, for instance, the detonation thicknesses even at ambient conditions are roughly of the order of $10 - 100\mu$m. As a result, grid sizes have to be sufficiently small in order for the details of the detonations to be captured. In the sequence of studies below, one-dimensional and two-dimensional detonating flows are used to establish baseline structure of the reactions before the periodic channel is discussed.

A. One-dimensional detonation structure

In the 1D configuration representing a homogeneous tube of length $L = 30$cm, fuel-air mixture is filled. The left boundary is set to a wall, while the right boundary is treated as an outflow. Near the left boundary, a small patch ($L_p = 30$ cm) is introduced. The grid size is set to $\Delta x = 2 \times 10^{-4}$m. Further details of this configuration are provided in [39].

The simulations were conducted for a set of cases involving methane and ethylene with varying degrees of hydrogen dilution. Table 1 summarizes the cases and key results. In the 1D case, one of the main model outputs is the detonation wave velocity, which can then be compared with the theoretical ZND-type calculation assuming equilibrium products [47]. It is seen that for the range of conditions considered here, the errors in the prediction of the theoretical speeed is within 1% for all cases considered. However, one of the cases, with 25% H_2 fails to detonate under the conditions specified. This is mainly due to the low detonability of methane. Note that in the theoretical computations, an equilibrium post-detonation solution is imposed, which ensures that a wave speed exists for these conditions. The pure CH_4 case is studied at higher pressure conditions with an initial pressure of 10 atm and initial temperature of 760K. These conditions are roughly comparable to post-compressor inflow conditions in gas turbines. For these conditions, a stable detonation is observed.

Since the 1D calculations used detailed chemical kinetics, the structure of the reaction zone can be analyzed in more detail. Figure 1 shows the species compositions relative to the location of the shock wave. Here, the shock wave is

Fuel(ratio)/Oxidizer	Computed CJ velosity	Thoretical CJ velocity	Error
CH_4/H_2(50/50)/ Air	1830 m/s	1836 m/s	0.33 %
CH_4/H_2(75/25)/ Air	N/A	1815 m/s	N/A
CH_4/H_2(25/75)/ Air	1870 m/s	1874 m/s	0.21 %
CH_4(10atm,760K)/ Air	1810 m/s	1816 m/s	0.88 %
C2H_4/ Air	1830 m/s	1824 m/s	0.33 %

Table 1 Chapman Jouget velocity comparison between computed values and theoretical values for CH_4 and C_2H_4 at 1 atm, 300K with air as oxidizer. dx = 0.2 mm.

identified as the location in the grid where the pressure is twice the baseline pressure. The two cases show comparable pressure profiles, with a sharp increase close to the shock wave leading to peak values of roughly 25 atm, before the flow expands and causes a drop in pressure to roughly 5 atm at 10 cm behind the shock wave. Both methane and ethylene are consumed in the early stages of detonation. It is also seen that CO production precedes CO_2, with the oxidation of CO occurring past the peak pressure for the methane case but before the peak pressure for the ethylene case. It is also interesting to note that the fuel and oxygen composition exhibit a gradual reduction in the initial phase (post shock wave) but undergo sudden rapid compression once a critical pressure is reached. For the ethylene case, this critical pressure is roughly 17 atm, while for the methane/hydrogen mixture this value is roughly 22 atm. It could be argued that this critical pressure is a measure of detonability, since the pressure peak is sustained by rapid heat release, which requires this rapid fuel/oxidizer consumption. As expected, the methane case shows a higher critical pressure in line with the lower detonability of methane.

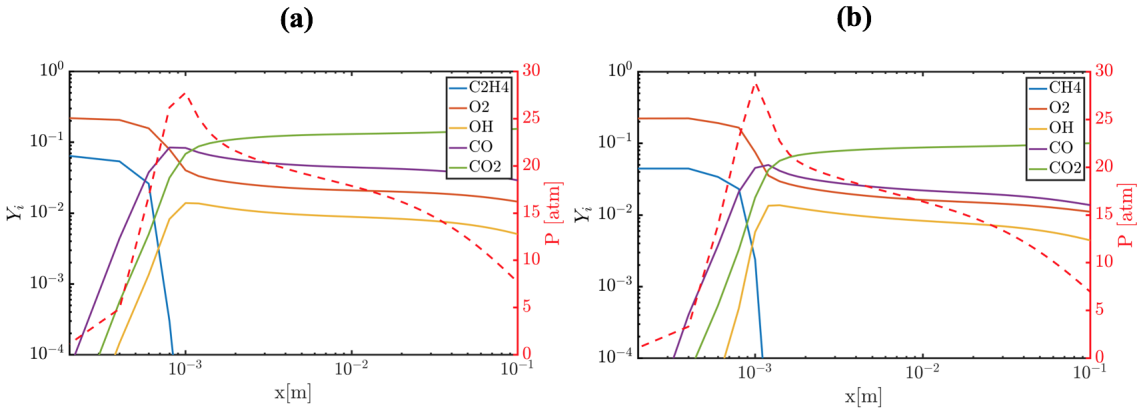

Fig. 1 Species and pressure in 1D detonation tube cases with a) pure C_2H_4, b) CH_4/H_2 = 50:50 in the reference of the shock front

B. Two-dimensional detonation simulations

Two dimensional computations involving detonations in confined channels are often used to characterize chemistry mechanisms based on the cellular structures formed in this process. Unlike the 1D configuration, the detonation process here is driven by formation of triple points and transverse waves that reflect from the top and bottom walls [48, 49].

The cellular structure is best visualized by plotting a time history of the peak pressure points within the domain, leading to the well known fish-scale pattern [48]. As a starting point, the soot foil record for ethylene/oxygen mixture is shown in Fig. 4. This condition has been previously studied by Araki et al. [16]. The computational domain consists of a channel of height h = 2mm and length $L = 2cm$. The grid size is set to $\delta x = 3 \times 10^{-6}$mm. The results from both studies are comparable, although the cellular structures in this present study are more regular. In addition, it is seen that longtitudinal waves emanate from the triple points, which is consistent with the prior work as well.

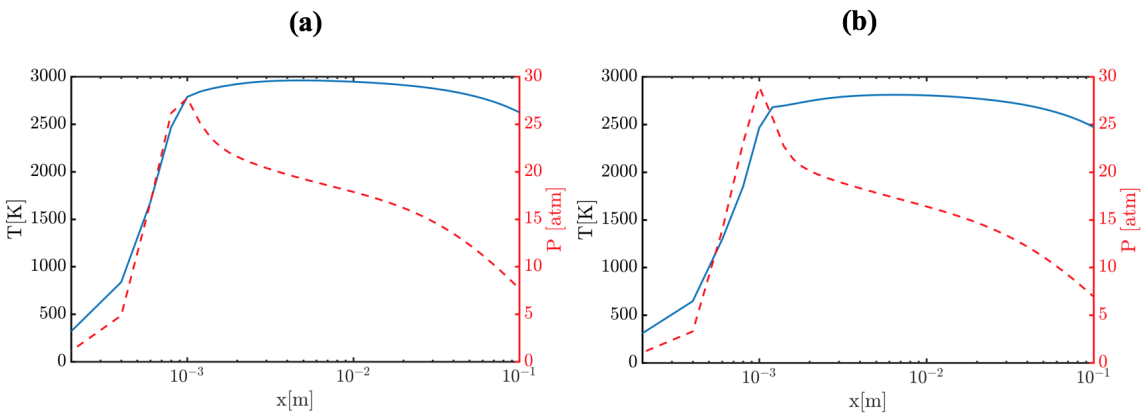

Fig. 2 Temperature and pressure profile in 1D detonation tube cases with a) pure C_2H_4, b) CH_4/H_2 = 50:50 in the reference of the shock front

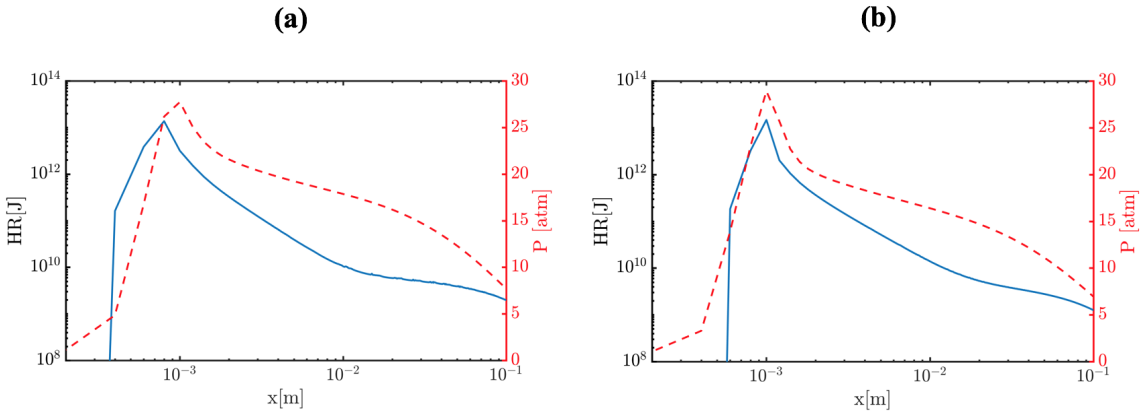

Fig. 3 Heat release and pressure profile in 1D detonation tube cases with a) pure C_2H_4, b) CH_4/H_2 = 50:50 in the reference of the shock front

Since methane mixtures are not highly detonable, the cell sizes as well as the domain size needed increase. For methane/hydrogen/air mixtures, the configuration is a channel of size 30cm × 5cm for a pre-detonation pressure of 1 atm and temperature of 300K. Three different mixtures of CH_4/H_2 at stoichiometric conditions are considered: a) 25:75, b) 50:50, c) 75:25. The detontability of the mixture decreases in that order as well. The grid size is set to $\Delta x = \Delta y = 2.2 \times 10^{-5}$m. The left and right boundary have zero gradient conditions imposed, while slip condition is used for the top and bottom boundary. A detonation wave is initiated by introducing a small high pressure region near the left boundary and creating artificial disturbances (by introducing small low pressure regions within the high pressure region) that lead to the formation of triple points [39].

Figure 5 shows the computed soot foil record for the three methane/hydrogen/air cases. It is seen that as the concentration of hydrogen increases, the cell sizes become smaller, consistent with the high reactivity of hydrogen. As the methane content increases, the cell structure become less regular and well-defined, with variations in cell sizes observed along the length of the channel. This is most likely due to the fact that some of the triple points do not sustain long enough to form the characteristic cell sizes. In addition, the pressure traces are thicker, implying that the detonation thickness is also larger than that for higher hydrogen content cases. Similar to the ethylene case, the lowest hydrogen content methane case exhibits longtitudinal waves, although it is less pronounced than in the ethylene/oxygen simulations. The only comparable calculation is that of Schwer and Kailasanath [17] where 50:50 methane/hydrogen was simulated. However, the cell sizes observed in those calculations were much different. The differences could be attributable to the chemistry mechanism used, since it was reported in that study that stable detonation could not achieved for 1D cases for this mixture (as opposed to the present study, where stable detonation structure was presented in Sec.A).

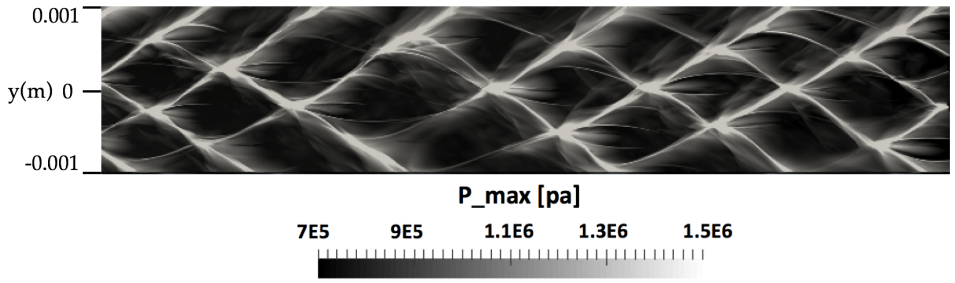

Fig. 4 Cell size comparison with C_2H_4. Channel height is 2 mm, dx = 3E-6m. The unburn mixture condition is 1 atm, 300K with O_2 as oxidizer.

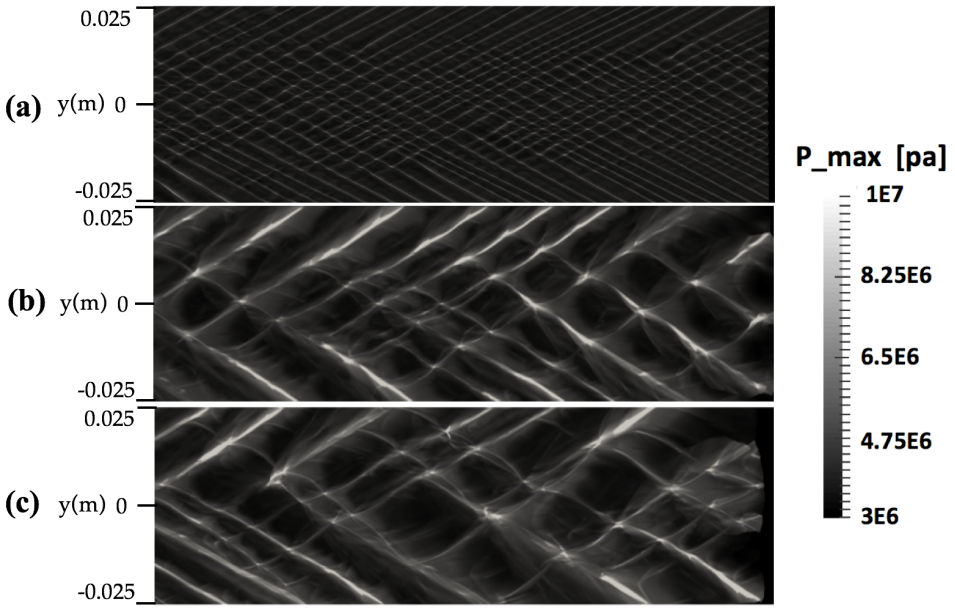

Fig. 5 Cell size comparison with different dilution ratio with H_2 for methane. Channel height is 5 cm, dx = 2.25E-5m. The unburn mixture condition is 1 atm, 300K with air as oxidizer. a) CH_4/H_2 = 25/75, b) CH_4/H_2 = 50/50, c) CH_4/H_2 = 75/25.

C. Two-dimensional RDE simulations

The one and two dimensional simulations discussed above showed some key asapects: a) there is a critical pressure required for hydrocarbon detonations to stay stable. This pressure is related to the pre-detonation pressure since that forms the baseline condition, but the critical pressure itself is fuel dependent; b) while methane mixtures are less likely to detonate, addition of hydrogen provides the necessary energy release to reach the critical pressure. However, methane mixtures show weaker detonation structures, reflected in the dissipation of triple points and thicker pressure traces. Based on these observations, the focus of the RDE simulations is to whether determine structural differences in detonation behavior is observed for different fuel/air mixtures at different operating conditions.

1. Flow configuration and computational details

The flow configuration considered is shown schematically in Fig. 6. The rectangular flow domain consists of periodic boundaries on the left and right side, and outflow at the top. At the bottom, premixed fuel-air mixture is injected based on prescribed stagnation conditions. A detonation wave is initiated by patching a one-dimensional solution in a small region of the domain. The flow then stabilizes over some initial time. All results presented here were extracted once a statistically stationary state is reached where the detonation wave travels at nearly constant speed across the domain. Fig. 6 also shows different flow features in the domain. In particular, the detonation wave seperates the reactant zone

from the product zone. As the product gases travel axially in the domain, they come in contact with fresh gases, leading to a region of possible deflagration. The flow then expands, gaining axial speed and reaches the outflow. Note that the nature of the outflow depends on the imposed back pressure. When the back pressure is relatively low (compared to post-detonation pressure), the flow will expand and can become supersonic. In this case, the numerically applied back pressure has no role in the simulations. On the other hand, if the back pressure is sufficiently large, the flow will be remain subsonic within the domain. The back pressure is an important quantity since it directly controls the pre-detonation pressure within the chamber. As a result, this variation in back pressure will be used to control the detonation processes in this work.

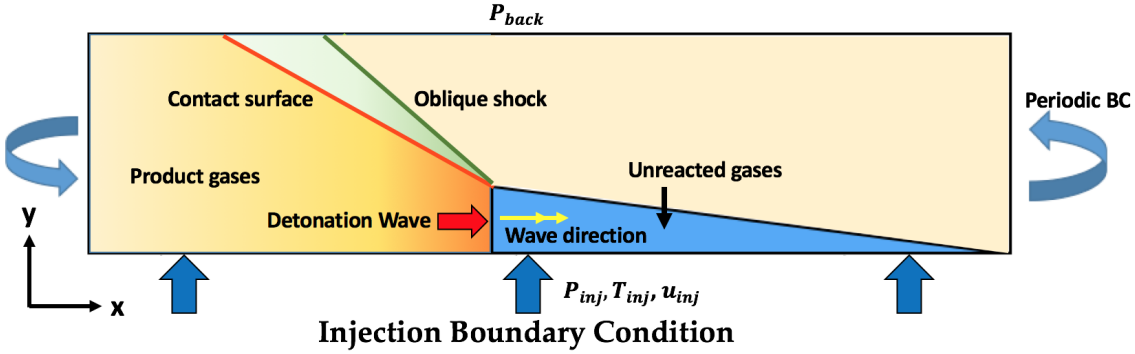

Fig. 6 General 2D unfolded RDEs configuration

The dimensions of the flow domain are based on prior studies [8, 17] and are provided in Table 2. While the geometry of Schwer and Kailasanath [17] is used to demonstrate validity of the current approach, the AFRL geometry is used to provide baseline data for future comparisons with experimental data. The grid spacing of 0.2mm is deemed sufficient for the calculations performed here. It was observed that reduction by a factor of 2-4 did not change the results.

Configuration	Geometry size [m]	Reference	Grid size	Grid spacing
1	$0.4788 \times 0.14 \times 0.01$	Schwer et al. [17]	1776348	2×10^{-4}m
2	$0.4596 \times 0.1016 \times 0.0076$	AFRL [8]	1263900	2×10^{-4}m

Table 2 Simulated domain size.

The prescription of the injection flux based on the chosen stagnation conditions require additional details. The method used here is identical to that of [50] but is repeated here for the sake of completeness. For this discussion P^0_{inj} indicates the stagnation pressure based on the injection conditions, P_{wall} is the pressure at the first control volume in the domain above the lower injection boundary, and P_{cr} denotes the critical pressure for choked flow based on the injection stagnation pressure and is computed as

$$P_{cr} = P^0_{inj}\left(\frac{2}{\gamma+1}\right)^{\frac{\gamma}{\gamma-1}}, \tag{6}$$

where γ is the specific-heat capacity ratio of the fuel-air mixture at the injection temperature prescribed.

As the detonation wave progresses in the domain, the pressure at the wall will change, with peak pressure associated with the detonation wave located in the control volume. The injection flux then depends on both on the inflow conditions and the conditions within the domain. Further, the flux depends on the location on the boundary and needs to be computed locally for each boundary control volume. For this reason, the injection flux is computed as follows:

- If $P_{wall} \geqslant P^0_{inj}$, the boundary cell face is treated as a wall.
- If $P^0_{inj} > P_{wall} > P_{cr}$, then the flow is not choked and $P_{inj} = P_{wall}$
- If $P_{wall} < P_{cr}$, then the flow is choked and $P_{inj} = P_{cr}$

Based on these conditions, the inflow quantities can be computed as

$$T_{inj} = T^0_{inj}\left(\frac{P_{inj}}{P^0_{inj}}\right)^{\frac{\gamma-1}{\gamma}}, \qquad u_{inj} = \sqrt{\frac{2\gamma}{\gamma-1}RT^0_{inj}\left[1-\left(\frac{P_{inj}}{P^0_{inj}}\right)^{\frac{\gamma-1}{\gamma}}\right]} \tag{7}$$

The flux computed based on the relations above is multiplied by an area ratio that denotes the ratio of cross-sectional area between the nozzles and the detonation chamber. This ratio is set to 0.2 for the present study. The outflow is treated either using supersonic or subsonic conditions based on the configuration. In this section, the outflow back pressure is set to be 1 atm as well. The grid is axially stretched near the exit plane in order to remove pressure fluctuations.

To obtain performance related metrics for the RDE, the mass flow rate is computed as

$$\dot{m} = \int_{inlet} \rho u_{inj} dx, \tag{8}$$

where ρ and u_{inj} are obtained from the boundary conditions discussed in Sec. III.C.1. The net force is obtained as

$$F = \int_{exit} \rho u^2 + (p - p_{back}) dx, \tag{9}$$

where p_{back} is the imposed back pressure, and u indicates the face-normal velocity. Based on these quantities, the specific impulse is computed as

$$I_{sp} = \frac{F}{\dot{m}_{fuel} g}, \tag{10}$$

where g is the gravitational acceleration and $\dot{m}_{fuel}$ is the mass of fuel in a total flow rate of $\dot{m}$.

The simulation results are also compared against analytical results, to provide a sanity check of the results. The analytical model used in this study is the axial flow model proposed by Shepherd et al. [51]. The basic assumption made in this model is that the flow becomes predominantly axial far away from the detonation layer. This assumption is valid if the injection does not have a net azimuthal rotation and a sufficiently long chamber makes azimuthal flow negligible at the exit [51]. It is shown that the following analytical relation for specific impulse can be derived by applying traditional rocket motor quasi-one-dimensional theory

$$\begin{aligned} \frac{F}{\dot{m}}\Big|_{P_{back}} &= a_1 f(M_{CJ}, \gamma, P_{back}/P_1) \\ &= a_1\sqrt{\frac{2}{\gamma-1}}\left[1 + \frac{1}{2(\gamma+1)}\left(M_{CJ} - \frac{1}{M_{CJ}}\right)^2 - \left(\frac{P_{back}}{P_1}\right)^{(\gamma-1)/\gamma}\frac{1}{M^2_{CJ}}\left(\frac{\gamma+1}{\gamma M^2_{CJ}+1}\right)^{-(\gamma+1)/\gamma}\right]^{1/2} \end{aligned} \tag{11}$$

where $\dot{m}$ is the mixture mass flow rate to the domain, a_1 is the speed of sound in the pre-detonation gases, M_{CJ} is the Mach number at CJ state, γ is the specific-heat ratio, P_{back} is the back pressure at the exit and P_1 is the pressure of the pre-detonation gases. The CJ state is computed in Cantera with inputs of pre-detonation conditions obtained in the simulation. Additional details about the model can be found in [51].

2. Comparison with prior RDE simulations

In order to verify the UMdetFOAM solver for periodic channel simulations, it is first compared against the geomtery of Schwer and Kailasanath [17], corresponding to configuration 1 in Table 2. Both hydrogen/air and ethylene/air at stoichiometric conditions with a temperature 300K and pressure of 1 atm were simulated.

Figure 7 shows the general flow field structure that exhibits the characteristic zones shown in the schematic (Fig. 6). The notations used by Kailasanath and Schwer [17] to mark the different regions of the flow. Region D denotes the detonation front which has a characteristic curved structure. The detonation front gives right to the oblique shock wave B The contact surface C exhibits strong shear-layer like features including vortical structures. The region G represents the unreacted gases that fill up, and the slope of the upper boundary between regions G and E is determined by the inflow flux and the speed of propagation of the detonation wave. In region F, injection is blocked due the high post detonation pressure, based on the boundary conditions discussed in Sec. III.C.1. Region E represents the burnt products which are convected from the detonation front in between the secondary shock wave D and the blocked injectors.

Table 3 shows the comparison of the results from the present study with both the simulations of Schwer and Kailasanath [17] and the theoretical model discussed above. Overall, the simulations in the current study compare well

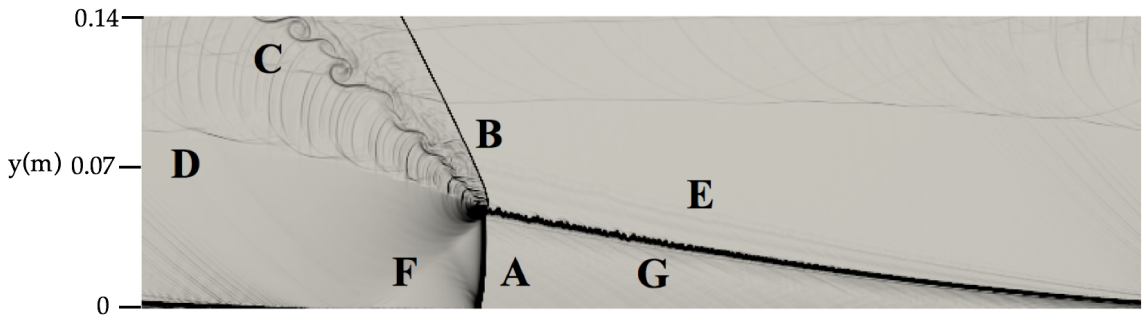

Fig. 7 General detonation structure visualized by the density gradient field obtained from the simulation with hydrogen/air detonation [52].

with the prior work, but produce higher force and specific impulse for all cases considered. The variations from the prior work observed here is consistent with the differences found by Schwer et al. [53] when using a new solver. Given that the mass flow rates are roughly equal, this implies that the outflow velocity and/or pressure are higher with the UMdetFOAM solver. This difference could be the result of numerical methods or due to differences in total heat release. The prior work uses an induction time based model which does not account for deflagration processes, especially at the boundaries separating regions G and E. Note that the simulations were conducted by setting viscosity and scalar diffusivities to zero, to be consistent with prior work [17]. However, the inclusion of these terms did not change the results significantly, as noted in the table. All simulations reported hereonafter use the viscous formulation.

Fuel	Model	Wave velocity[m/s]	Mass flow [kg/s]	F [N]	I_{sp} [1/s]
H_2	Detailed kinetics/Euler	1927	1.611	2319	5186
H_2	IPM	1854	1.613	2199	4911
H_2	Analytical	1984	–	–	5463
C_2H_4	Detailed kinetics/Euler	1780	1.866	2513	2158
C_2H_4	IPM	1716	1.877	2364	2022
C_2H_4	Analytical	1838	–	–	2357
C_2H_4	Detailed kinetics/Navier Stokes	1781	1.867	2511	2155

Table 3 Comparison between present study, prior RDE simulations of Schwer and Kailasanath [17] and theoretical model [51]. The oxidizer is air. P^0_{inj}=10 atm, T^0_{inj}=300 K, P_{back} = 1 atm

3. RDE simulations with hydrocarbon mixtures

The cases studied in this section are based on the AFRL geometry (configuration 2 in Tab. 2). The full viscous/diffusive terms are included in the simulations. The cases considered include ethylene and methane with varying degrees of dilution as well as varying operating conditions. A list of mixtures and operating conditions are provided in Table 4. Since pure methane does not detonate at ambient inflow conditions, higher injection and back pressure as well as increased inflow temperature were considered.

For both of the ethylene and methane chemistry, the wave speed and the specific impulse increases with high dilution ratio with hydrogen while thrust decreases. Since hydrogen is more detonable and exhibits a higher CJ speed, this trend indicates that the heat release process is increasingly dominated by the presence of hydrogen. For the methane/hydrogen 50:50 blend, it is seen that as the back pressure increases, the thrust decreases, which is consistent with the definition of thrust in Eq. 9. Further, the specific impulse also decreases as the ratio of the injection stagnation pressure to back pressure increases. As will be seen in the detailed images of flow field, this reduction comes mainly through a reduction in the acceleration of the flow processed by the detonation wave. When the back pressure is low, the flow becomes supersonic while with increasing back pressure, the flow remains subsonic. This reduction is velocity is achieved

through tertiary shock waves that reduce the total pressure of the fluid. While thi numerical thrust is lower, it could be expected that in a practical device, the flow would expand and a direct comparison at downstream location for identical pressure conditions need to be obtained. Further study is needed to determine a robust approach for comparing exit thrust calculations.

The comparisons with theoretical specific impulse predictions show interesting trends. For large P^0_{inj}/P_{back}, the detailed calculations and the theoretical predictions are reasonably close, indicating that when the flow is expanded to supersonic conditions, the assumptions underpinning the theoretical model are valid. However, when the back pressure is increased, the differences become large, since the flow at the exit plane is subsonic and might contain significant azimuthal component to the flow.

Mixture	$P^0_{inj} : P_{back} : T^0_{inj}$ [atm]:[atm];[K]	Wave velocity [m/s]	Th.Wave velocity [m/s]	Mass flow [kg/s]	F [N]	I_{sp} [1/s]	Th.I_{sp} [1/s]
C_2H_4	10:1:300	1786	1837	1.362	1832	2156	2314
C_2H_4/H_2(75/25)	10:1:300	1798	1845	1.35	1824	2228	2519
C_2H_4/H_2(50/50)	10:1:300	1820	1858	1.327	1808	2362	2651
C_2H_4/H_2(25/75)	10:1:300	1854	1885	1.285	1778	2702	2987
CH_4/H_2(75/25)	30:6:300	N/A	N/A	N/A	N/A	N/A	N/A
CH_4/H_2(50/50)	30:6:300	1760	1864	3.881	4494	2370	2520
CH_4/H_2(75/25)	30:10:793	N/A	N/A	N/A	N/A	N/A	N/A
CH_4/H_2(50/50)	30:10:793	1697	1846	2.642	1909	1479	1760
CH_4	30:14:793	1685	1817	2.618	1537	1086	1482
CH_4/H_2(75/25)	30:14:793	1699	1830	2.601	1517	1122	1577
CH_4/H_2(50/50)	30:14:793	1723	1850	2.572	1496	1191	1675
CH_4/H_2(25/75)	30:14:793	1754	1887	2.515	1447	1342	1918

Table 4 Global results and analytical values for each case

The details of the flow field are provided in Fig. 8-11, where temperature and pressure fields from the ethylene/hydrogen and methane/hydrogen simulations are provided. The temperature plots show that the overall structure of the detonation wave does not change between the different simulations. However, for both ethylene and methane, the pure fuel simulations produce lower temperatures in the region between the contact surface and the oblique shock wave. As the hydrogen content is increased, the temperature in this region increases. For the methane case, tertiary shock structures appear, leading to striations in the temperature field. The pressure field shows similar behavior, with the pure fuel cases providing higher pressure jumps across the detonation front. Moreover, the detonation height, defined as the distance from the bottom of the domain to the highest axial point at which peak detonation pressure is observed, is found to decrease with increase in hydrogen concentration. As the hydrogen content is increased, the detonation wave speed increases, but the injection flux is still controlled by the higher density hydrocarbon content. As a result, the refill height decreases leading to shorter detonation height.

An important feature of the flow is the acceleration of subsonic or sonic incoming flow to supersonic speeds, subject to the effect of backpressure. Figures 12 and 13 show the Mach number field for the two sets of cases. The ethylene cases show remarkably similar Mach number fields, implying that the flow behavior is not substantially altered by the addition of hydrogen. Much of the flow is accelerated to roughly Mach 2, which is roughly the CJ speed expressed in terms of the speed of sound post detonation. Note that the ethylene cases exit to ambient conditions. On the other hand, the methane simulations show a more complex behavior. Due to the higher back pressure, the flow is restricted by tertiary shock structures that increase the static pressure (and temperature) while reducing the flow velocity. This is very clearly seen in the $P_{back} = 6$ atm case, which exhibits multiple shock structures in the post detonation region. As the back pressure is further increased, the baseline pressure inside the combustor is higher, and the flow remains subsonic except near the contact surface and the detonation front itself. It is important to note that the pressure is not merely scaled when the back pressure is increased, but the flow itself is fundamentally altered.

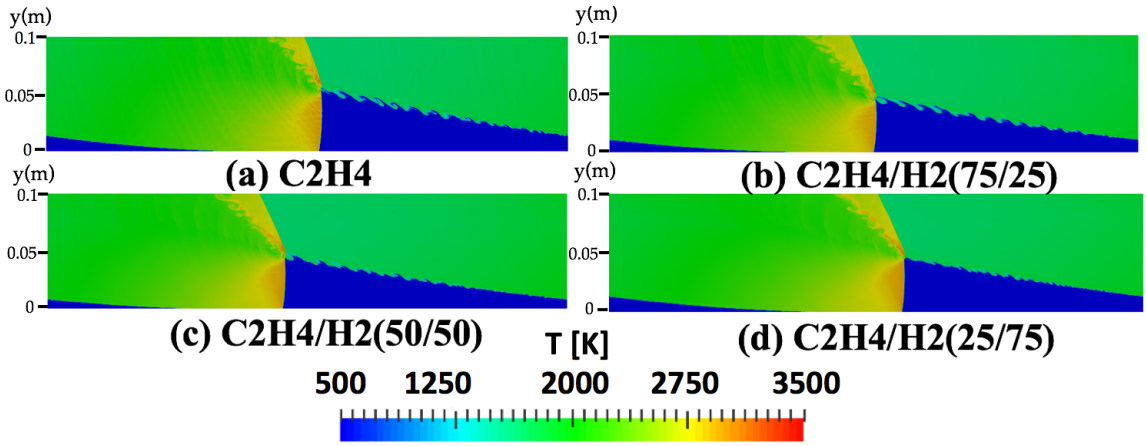

Fig. 8 Temperature field for C_2H_4 with different dilution ratio with H_2

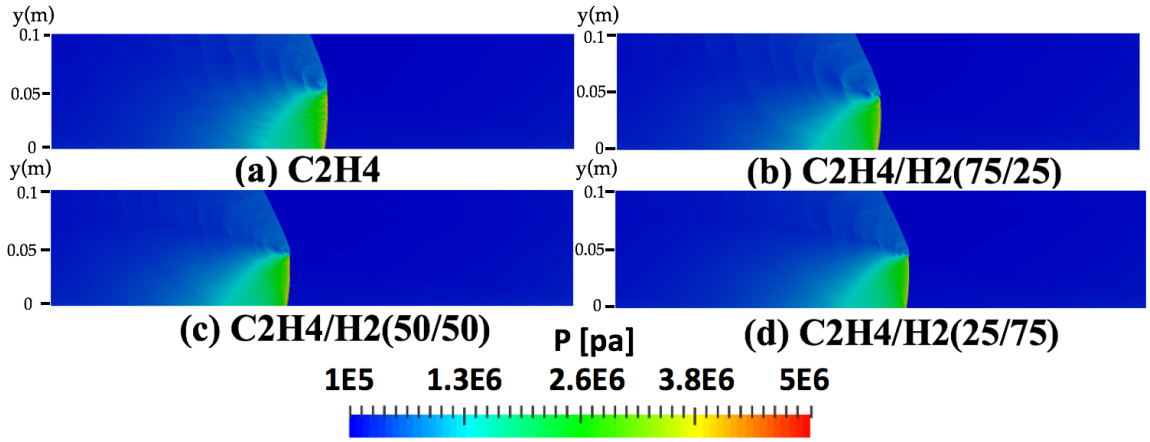

Fig. 9 Pressure field for C_2H_4 with different dilution ratio with H_2

Further analysis is conducted using one dimensional profiles, extracted normal to the detonation front. Figure 14 shows the pressure profile across the detonation front for the two fuel mixtures, obtained at a height of 1cm above the bottom wall. It is seen that for ethylene cases that have low back pressure, the pre-detonation pressure is slightly higher than 1 atm, while for the methane cases, due to the high back pressure, this pre-detonation condition is closer to the back pressure value. As a result, the pressure increase across the detonation front is higher, which reduces the ignition delay time and leads to a stable detonation wave. Further, the pre-detonation pressure is invariant with distance from detonation front for the ethylene cases, but the increased back pressure leads to a change in pressure roughly 5mm ahead of the wave. It should be noted that when the back pressure is large, the flow can become unchoked leading to a reduction in mass flow rate. Figure 15 shows the peak pressure as a function of hydrogen content in the mixture. For the ethylene case, addition of hydrogen only leads to a 11% decrease in peak pressure but for methane, an approximate 25% reduction is seen. As the peak pressure decreases, the initial acceleration of the flow past the shock wave is reduced, leading to lower Mach numbers post shock-wave.

Figure 17 shows the fraction of heat release at a particular pressure range behind the detonation wave. It is seen that for the ethylene cases, the peak fraction of heat release occurs in the 35-40 atm pressure range, and is relatively unchanged with addition of hydrogen. However, for methane, the peak heat release farction switches from the 80-100 atm range to 60-80 atm range as the hydrogen content increases. Further, pure methane shows heat release at even higher pressures of 120-140 atm. Figure 3 shows the same heat release fraction but for a one-dimensional detonation wave for the pure ethylene and methane cases. Interestingly, the 1D case contains two peaks in heat release fraction for ethylene and a heat releaes fraction at lower pressure for methane. This indicates that the expansions behind the detonation wave as well as the interaction with the other regions in the domain alters the wave properties. Hence, a

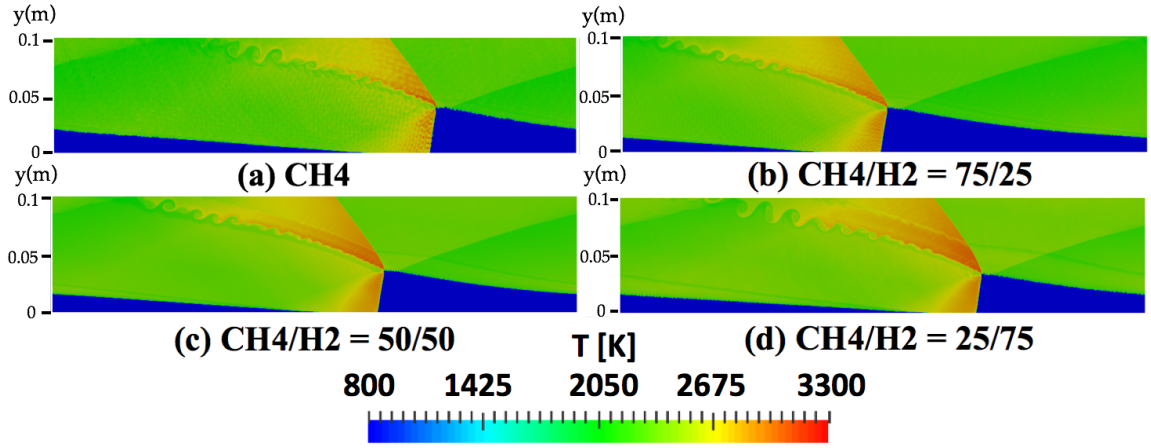

Fig. 10 Temperature field for CH_4 cases with $P0_{inj} : P_{back} : T0_{inj}$ = 30atm:14atm:793K

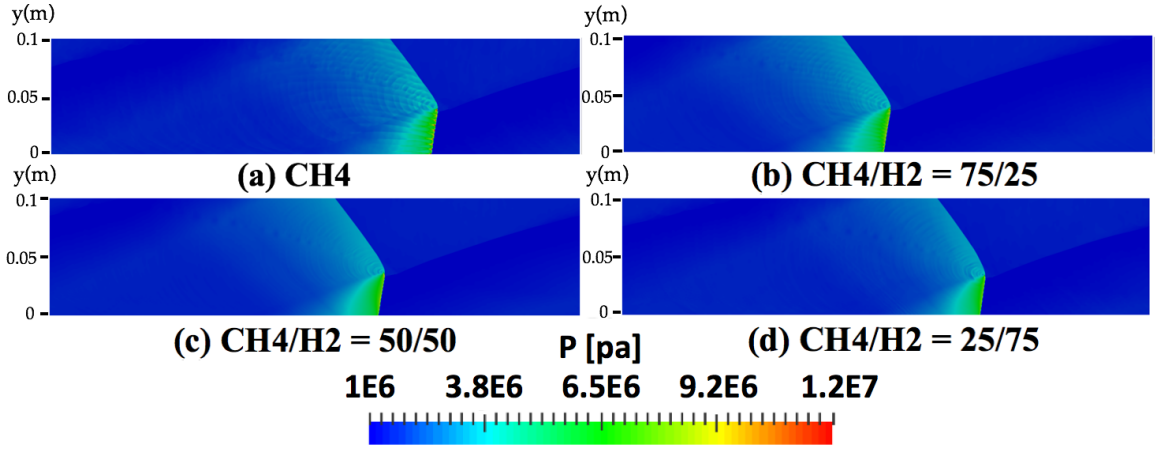

Fig. 11 Pressure field for CH_4 cases with $P0_{inj} : P_{back} : T0_{inj}$ = 30atm:14atm:793K

direct use of one-dimensional models for predicting even two-dimensional detonation waves may not be accurate.

Finally, the species profiles across the detonation front are shown in Fig. 18 for the pure ethylene and methane cases. The profiles are remarkably similar to Fig. 1, with the initial decomposition of fuel molecules followed by sudden consumption once a critical pressure is reached. Similarly the CO oxidation occurs after the pressure peak and continues, albeit at a slow rate with substantial CO remaining even after 1cm past the detonation front. Figure 19 shows Mach number, pressure and normalized temperature contours, which also show similar behavior to one-dimensional detonation wave profiles (Fig. 2). Interestingly, the flow is first accelerated to supersonic speeds right behind the shock front before expansion reduces the temperature and the flow speed. Note that the acceleration of the flow occurs in an oblique direction while these profiles are obtained normal to the wave front which is nearly aligned with the coordinate directions.

IV. Summary and Conclusions

A detailed kinetics solver is used to study detonations of various hydrocarbon/hydrogen mixtures in air at a range of operating conditions has been studied. The simulations were validated extensively by comparison against theoretical results and prior work available in literature. A two-dimensional periodic channel representing an unwrapped RDE configuration was used to understand the role of operating conditions and fuel composition on detonation structure. The simulations yielded the following conclusions:

- While pure ethylene detonates at pre-detonation conditions corresponding to 1 atm and 300K, methane requires

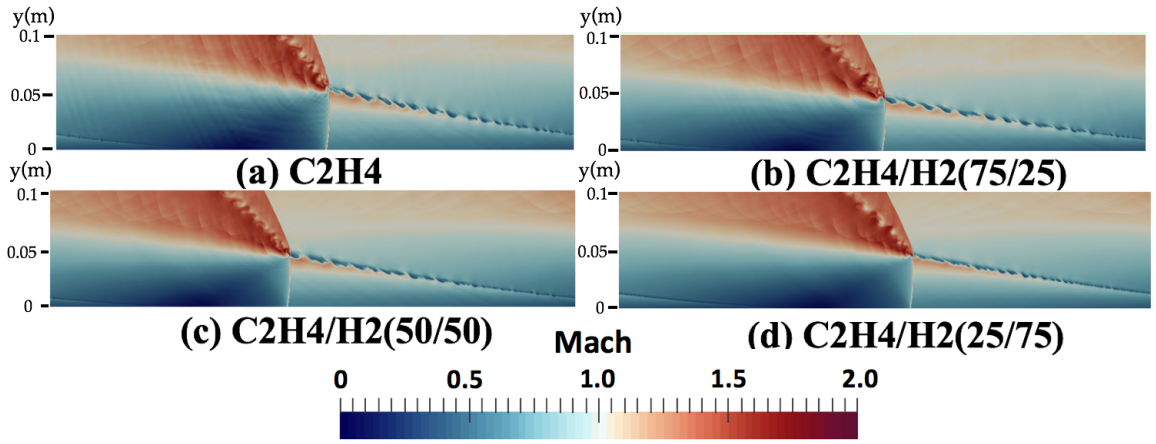

Fig. 12 Mach number field for C_2H_4 with different dilution ratio with H_2

higher pressure and inflow temperature. As expected, the addition of hydrogen increaseses the detonability.

- The back pressure specified at the exit plane of the combustor determine the pre-detonation pressure. As a result, higher back pressure values lead to increased detonability, but also restricts the acceleration of the post-detonation products causing the velocity in these regions to remain subsonic. In some cases, such high back pressure led to the formation of tertiary shock waves needed to additionally compress the flow in order to match the exit plane conditions.
- The detonation wave-normal profiles match the one-dimensional detonation simulation results, with a strong post-detonation pressure peak followed by a decay in pressure. The fluid is compressed and accelerated past the shock wave. It is observed that methane produces higher peak pressure near the detonation front, and this pressure decreases by nearly 25% with addition of 75% hydrogen. The peak pressure for ethylene is considerably lower and does not show significant variation with hydrogen addition.
- The heat release behind the shock wave occurs predominantly when the pressure reaches 35-40 atm (ethylene cases) or 80-100 (methane cases). However, addition of hydrogen reduces the heat release pressure to 60-80 atm in the methane case but exhibits no significant change fo the ethylene case.

These findings have provided additional insight into the detonation structure by including detailed kinetics information. The next step will be to use this detailed kinetics approach to simulate full-scale three-dimensional RDE configurations. This work is currently being pursued.

V. Acknowledgement

The authors gratefully acknowledge financial support from DOE-NETL through grant DE-FE0025315 with Dr. Mark Freeman as program monitor. The authors are grateful for the generous allocation of computational resources on the NCSA Blue Waters System.

References

[1] Zhou, R., Wu, D., and Wang, J., "Progress of continuously rotating detonation engines," *Chinese Journal of Aeronautics*, Vol. 29, No. 1, 2016, pp. 15–29.

[2] Kailasanath, K., "The rotating-detonation-wave engine concept: a brief status report," *49th AIAA Aerospace Sciences Meeting*, 2011, pp. 2011–0580.

[3] Cullen, R., Nicholls, J., and Ragland, K., "Feasibility studies of a rotating detonation wave rocket motor." *Journal of Spacecraft and Rockets*, Vol. 3, No. 6, 1966, pp. 893–898.

[4] Voitsekhovskii, B. V., "A spin stationary detonation," *Applied Mechanics and Technical Physics*, Vol. 3, 1960, pp. 157–164.

[5] Tsuboi, N., Watanabe, Y., Kojima, T., and Hayashi, A. K., "Numerical estimation of the thrust performance on a rotating detonation engine for a hydrogen–oxygen mixture," *Proceedings of the Combustion Institute*, Vol. 35, No. 2, 2015, pp. 2005–2013.

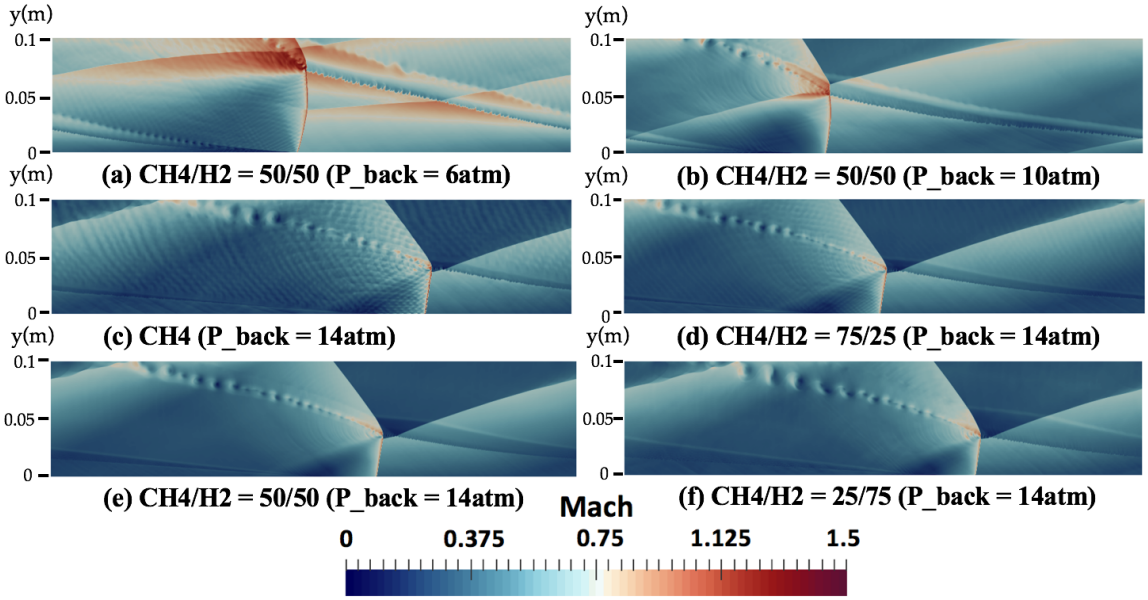

Fig. 13 Mach number field for CH_4

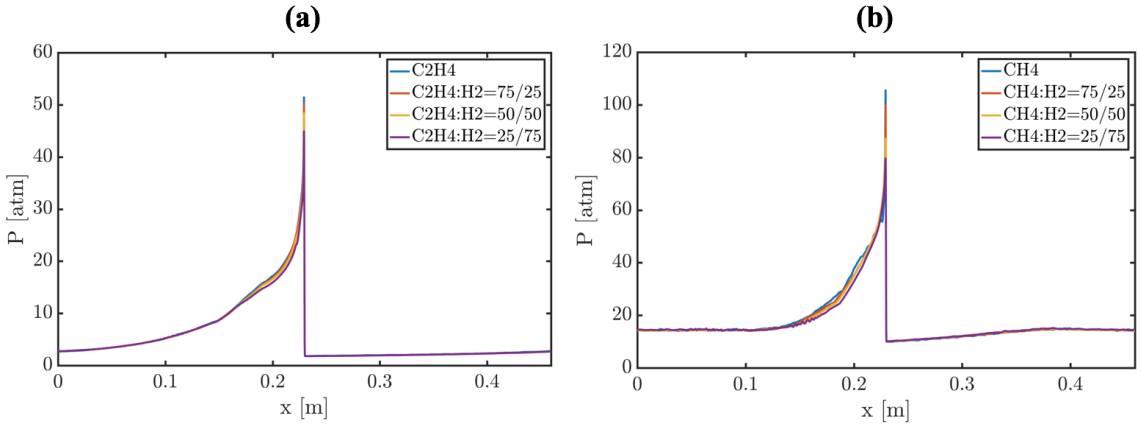

Fig. 14 Averaged pressure profile for a) C_2H_4 and b) CH_4 at 1cm above from the bottom boundary

[6] Schwer, D., and Kailasanath, K., "Numerical investigation of the physics of rotating-detonation-engines," *Proceedings of the Combustion Institute*, Vol. 33, No. 2, 2011, pp. 2195–2202.

[7] Rankin, B. A., Richardson, D. R., Caswell, A. W., Naples, A. G., Hoke, J. L., and Schauer, F. R., "Chemiluminescence imaging of an optically accessible non-premixed rotating detonation engine," *Combustion and Flame*, Vol. 176, 2017, pp. 12–22.

[8] Rankin, B. A., Richardson, D. R., Caswell, A. W., Naples, A., Hoke, J. L., and Schauer, F. R., "Imaging of OH* chemiluminescence in an optically accessible nonpremixed rotating detonation engine," *53rd AIAA Aerospace Sciences Meeting*, 2015, pp. 2015–1604.

[9] Anand, V., George, A. S., Driscoll, R., and Gutmark, E., "Analysis of air inlet and fuel plenum behavior in a rotating detonation combustor," *Experimental Thermal and Fluid Science*, Vol. 70, 2016, pp. 408–416.

[10] Anand, V., George, A. S., and Gutmark, E., "Amplitude modulated instability in reactants plenum of a rotating detonation combustor," *International Journal of Hydrogen Energy*, Vol. 42, No. 17, 2017, pp. 12629–12644.

[11] Rhee, H., Ishiyama, C., Higashi, J., Kawasaki, A., Matsuoka, K., Kasahara, J., Matsuo, A., and Funaki, I. F., "Experimental Study on a Rotating Detonation Turbine Engine with an Axial Turbine," *26th International Colloquium on the Dynamics of Explosions and Reactive Systems*, 2017.

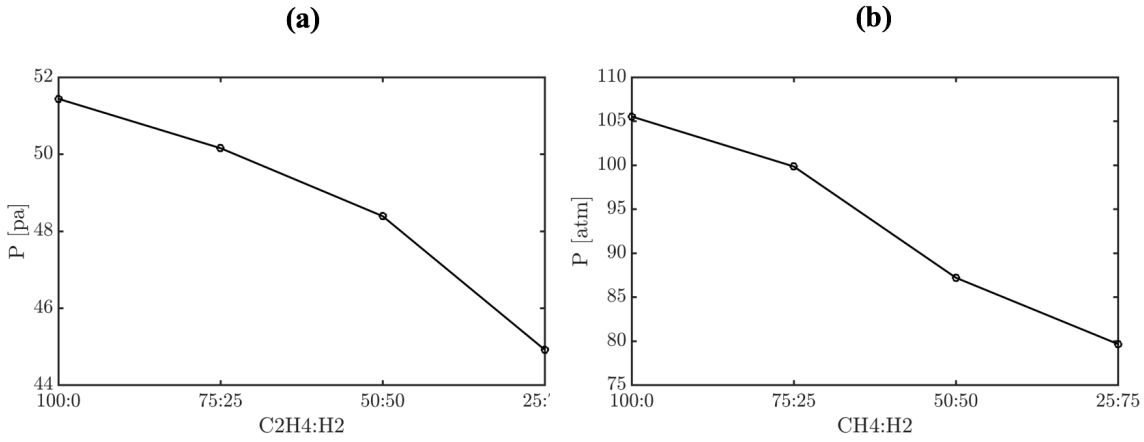

Fig. 15 Averaged peak pressure for a) C_2H_4 and b) CH_4 at 1 cm above from the bottom boundary

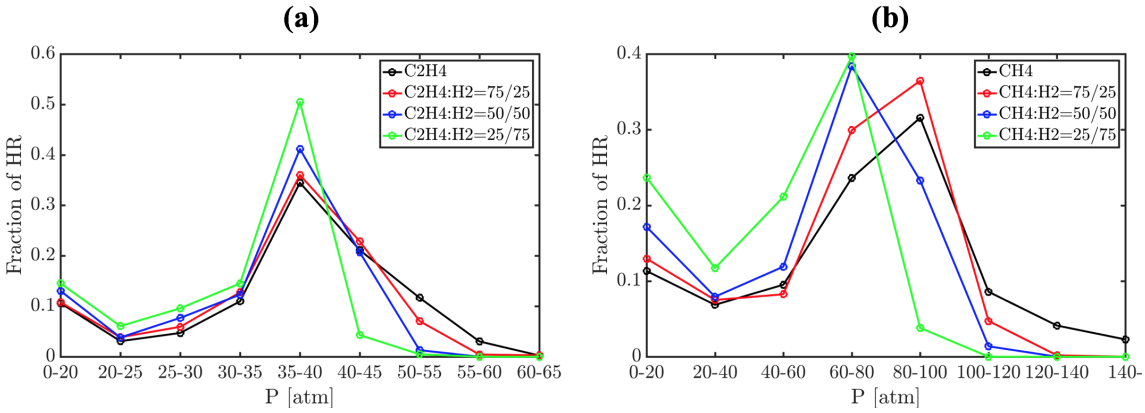

Fig. 16 Heat release fraction VS. pressure for a) C_2H_4 and b) CH_4 cases with $P0_{inj}$: P_{back} : $T0_{inj}$ = 30atm:14atm:793K

[12] Kindracki, J., Wolański, P., and Gut, Z., "Experimental research on the rotating detonation in gaseous fuels–oxygen mixtures," *Shock waves*, Vol. 21, No. 2, 2011, pp. 75–84.

[13] Lentsch, A., Bec, R., Serre, L., Falempin, F., Daniau, E., Piton, D., Prigent, A., Canteins, G., Zitoun, R., Desbordes, D., et al., "Overview of current French activities on PDRE and continuous detonation wave rocket engines," *AIAA*, Vol. 3232, 2005, p. 2005.

[14] Wang, Y., Wang, J., Li, Y., and Li, Y., "Induction for multiple rotating detonation waves in the hydrogen–oxygen mixture with tangential flow," *International Journal of Hydrogen Energy*, Vol. 39, No. 22, 2014, pp. 11792–11797.

[15] Shank, J. C., King, P. I., Karnesky, J., Schauer, F., and Hoke, J. L., "Development and testing of a modular rotating detonation engine," *50th AIAA Aerospace Sciences Meeting*, 2012, pp. 2012–0120.

[16] Araki, T., Yoshida, K., Morii, Y., Tsuboi, N., and Hayashi, A. K., "Numerical analyses on ethylene/oxygen detonation with multistep chemical reaction mechanisms: Grid resolution and chemical reaction model," *Combustion Science and Technology*, Vol. 188, No. 3, 2016, pp. 346–369.

[17] Schwer, D. A., and Kailasanath, K., "Assessment of Rotating Detonation Engines with Fuel Blends," *53rd AIAA/SAE/ASEE Joint Propulsion Conference*, 2017, p. 4942.

[18] Schwer, D., and Kailasanath, K., "Fluid dynamics of rotating detonation engines with hydrogen and hydrocarbon fuels," *Proceedings of the Combustion Institute*, Vol. 34, No. 2, 2013, pp. 1991–1998.

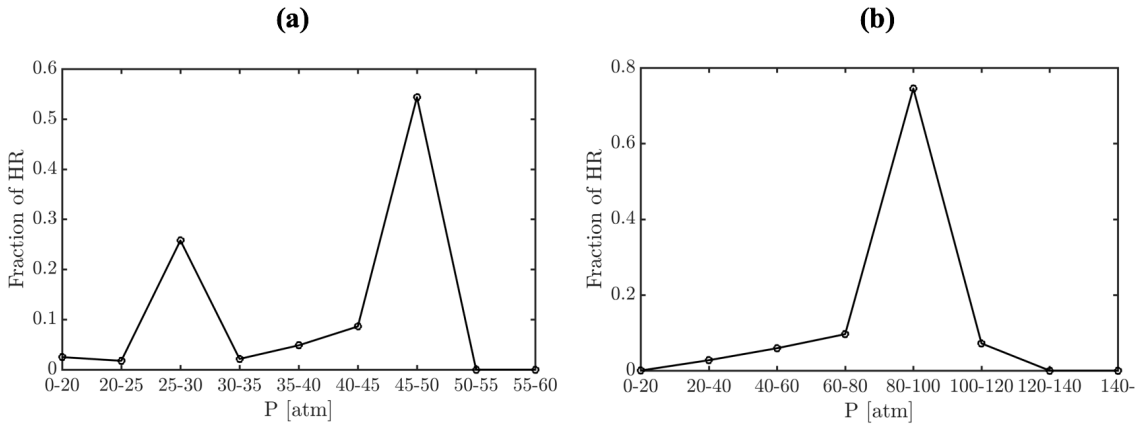

Fig. 17 Heat release fraction VS.pressure in the 1D configuration for a) C_2H_4 and b) CH_4 cases with $P0_{inj}$: P_{back} : $T0_{inj}$ = 10atm:1atm:300K and 30atm:14atm:792.79K, respectively

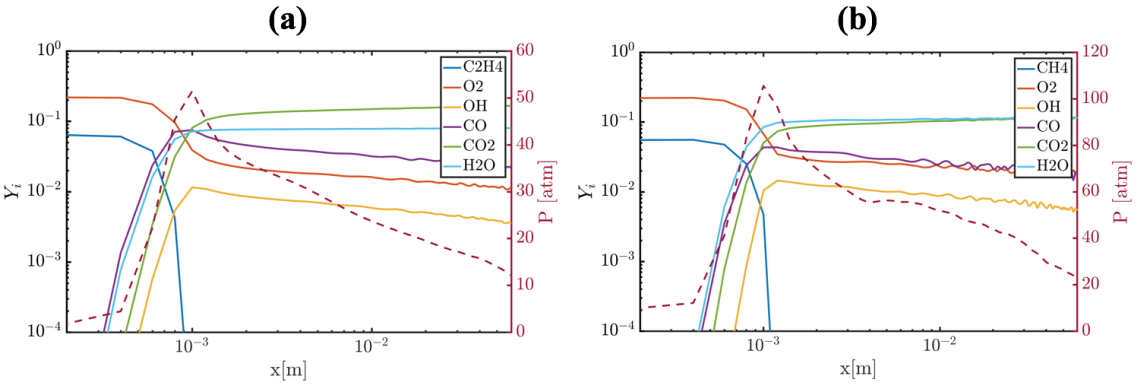

Fig. 18 Species and pressure profile for a) pure C_2H_4, b) pure CH_4 cases at the detonation front in the reference of the shock front at 1cm above from the bottom boundary

[19] Mével, R., Davidenko, D., Lafosse, F., Chaumeix, N., Dupré, G., Paillard, C.-É., and Shepherd, J. E., "Detonation in hydrogen–nitrous oxide–diluent mixtures: An experimental and numerical study," *Combustion and Flame*, Vol. 162, No. 5, 2015, pp. 1638–1649.

[20] Stechmann, D. P., Heister, S. D., and Sardeshmukh, S. V., "High-pressure rotating detonation engine testing and flameholding analysis with hydrogen and natural gas," *55th AIAA Aerospace Sciences Meeting*, 2017, p. 1931.

[21] Wolański, P., Kauffman, C., Sichel, M., and Nicholls, J., "Detonation of methane-air mixtures," *Symposium (International) on Combustion*, Vol. 18, Elsevier, 1981, pp. 1651–1660.

[22] Burr, J., and Yu, K., "Detonation Wave Propagation in an Open Channel with Transverse Jets," *53rd AIAA/SAE/ASEE Joint Propulsion Conference*, 2017, p. 4908.

[23] Fotia, M., Hoke, J., and Schauer, F., "Propellant plenum dynamics in a two-dimensional rotating detonation experiment," *52nd aerospace sciences meeting*, 2014, p. 1013.

[24] Davidenko, D., Gökalp, I., and Kudryavtsev, A., "Numerical study of the continuous detonation wave rocket engine," *15th AIAA International Space Planes and Hypersonic Systems and Technologies Conference*, 2008, p. 2680.

[25] Schwer, D., and Kailasanath, K., "Feedback into mixture plenums in rotating detonation engines," *50th AIAA Aerospace Sciences Meeting including the New Horizons Forum and Aerospace Exposition*, 2012, p. 617.

[26] Schwer, D., and Kailasanath, K., "Effect of inlet on fill region and performance of rotating detonation engines," *47th AIAA/ASME/SAE/ASEE Joint Propulsion Conference & Exhibit*, 2011, p. 6044.

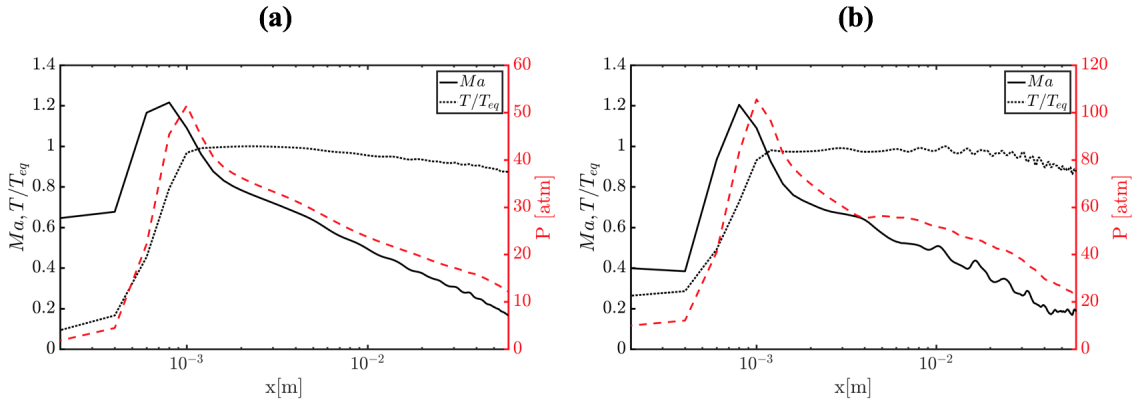

Fig. 19 Mach number and temperature profile for a) pure C_2H_4, b) pure CH_4 case at the detonation front in the reference of the shock front at 1cm above from the bottom boundary

[27] Schwer, D., Corrigan, A., Taylor, B., and Kailasanath, K., "On reducing feedback pressure in rotating detonation engines," *51st AIAA Aerospace Sciences Meeting including the New Horizons Forum and Aerospace Exposition*, 2013, p. 1178.

[28] Varatharajan, B., Petrova, M., Williams, F., and Tangirala, V., "Two-step chemical-kinetic descriptions for hydrocarbon–oxygen-diluent ignition and detonation applications," *Proceedings of the Combustion Institute*, Vol. 30, No. 2, 2005, pp. 1869–1877.

[29] Li, S., Varatharajan, B., and Williams, F., "The chemistry of ethylene ignition for application to pulse-detonation engines," *36th AIAA/ASME/SAE/ASEE Joint Propulsion Conference and Exhibit*, 2000, p. 3475.

[30] Li, C., Kailasanath, K., and Oran, E. S., "Detonation structures behind oblique shocks," *Physics of Fluids*, Vol. 6, No. 4, 1994, pp. 1600–1611.

[31] Gamezo, V. N., Desbordes, D., and Oran, E., "Two-dimensional reactive flow dynamics in cellular detonation waves," *Shock Waves*, Vol. 9, No. 1, 1999, pp. 11–17.

[32] Yao, S., Tang, X., Luan, M., and Wang, J., "Numerical study of hollow rotating detonation engine with different fuel injection area ratios," *Proceedings of the Combustion Institute*, Vol. 36, No. 2, 2017, pp. 2649–2655.

[33] Shimizu, H., Tsuboi, N., and Hayashi, A., "Study of detailed chemical reaction model on hydrogen–air detonation," *39th AIAA aerospace sciences meeting and exhibit, Reno, AIAA paper*, Vol. 478, 2001, p. 2001.

[34] Gaillard, T., Davidenko, D., and Dupoirieux, F., "Numerical Simulation of a Rotating Detonation under Conditions of Premixed and Separate Injection of H2- O2," 2017.

[35] Fievisohn, R. T., and Yu, K. H., "Parametric Study of an Ethylene-Air Rotating Detonation Engine Using an Ideal Model," *54th AIAA Aerospace Sciences Meeting*, 2016, p. 1403.

[36] Wilhite, J., Driscoll, R. B., St. George, A. C., Anand, V., and Gutmark, E. J., "Investigation of a rotating detonation engine using ethylene-air mixtures," *54th AIAA Aerospace Sciences Meeting*, 2016, p. 1650.

[37] "The Open Source CFD Toolbox http://openfoam.org," , 2016. URL `http://openfoam.org`.

[38] Damien Masselot, S. V., Takuma Sato, and Raman., V., "Development of Robust Computational Tools for Rotating Detonation Engines," *10th Mediterranean Combustion Symposium*, 2018.

[39] Sato, T., Voelkel, S., and Raman, V., "Detailed Chemical Kinetics based Simulation of Detonation Containing Flows," , 2018. Submitted to ASME Turbo Expo.

[40] Toro, E. F., Spruce, M., and Speares, W., "Restoration of the contact surface in the HLL-Riemann solver," *Shock Waves*, Vol. 4, No. 1, 1994, pp. 25–34. doi:10.1007/BF01414629.

[41] Toro, E. F., *Riemann Solvers and Numerical Methods for Fluid Dynamics: A Practical Introduction*, Springer, 2009.

[42] Greenshields, C. J., Weller, H. G., Gasparini, L., and Reese, J. M., "Implementation of semi-discrete, non-staggered central schemes in a colocated, polyhedral, finite volume framework, for high-speed viscous flows," *International journal for numerical methods in fluids*, Vol. 63, No. 1, 2010, pp. 1–21.

[43] Goodwin, D., Malaya, N., Moffat, H., and Speth, R., "Cantera: An Object Oriented Software Toolkit for Chemical Kinetics, Themodynamics, and Transport Processes, Version 2.1.1," , 2012.

[44] Varatharajan, B., and Williams, F., "Ethylene ignition and detonation chemistry, part 2: Ignition histories and reduced mechanisms," *Journal of Propulsion and Power*, Vol. 18, No. 2, 2002, pp. 352–362.

[45] Petersen, E. L., and Hanson, R. K., "Reduced kinetics mechanisms for ram accelerator combustion," *Journal of Propulsion and power*, Vol. 15, No. 4, 1999, pp. 591–600.

[46] Powers, J., and Paolucci, S., "Accurate spatial resolution estimates for reactive supersonic flow with detailed chemistry," *AIAA JOURNAL*, Vol. 43, No. 5, 2005, pp. 1088–1099. doi:{10.2514/1.11641}, AIAA 43rd Aerospace Sciences Meeting and Exhibit, Reno, NV, JAN 10-13, 2005.

[47] "Shock Detonation Toolbox: http://shepherd.caltech.edu," , 2014. URL `http://shepherd.caltech.edu/EDL/public/cantera/html/SD_Toolbox/#Notes`.

[48] Oran, E. S., Weber., J. W., Stefaniw, E. I., Lefebvre, M. H., and Anderson., J. D., "A Numerical Study of a Two-Dimensional H2-O2-Ar Detonation Using a Detailed Chemical Reaction Model," *Combust. Flame*, Vol. 113, No. 1–2, 1998, pp. 147 – 163. doi:http://dx.doi.org/10.1016/S0010-2180(97)00218-6.

[49] Irvin Glassman, N. G. G., Richard A. Yetter, *Combustion, Fifth Edition*, Academic Press, 2014.

[50] Schwer, D., and Kailasanath, K., "Numerical investigation of rotating detonation engines," *46th AIAA/ASME/SAE/ASEE Joint Propulsion Conference & Exhibit*, 2010, p. 6880.

[51] Shepherd, J. E., and Kasahara, J., "Analytical Models for the Thrust of a Rotating Detonation Engine," 2017.

[52] Mueller, M., Kim, T., Yetter, R., and Dryer, F., "Flow reactor studies and kinetic modeling of the H2/O2 reaction," *International Journal of Chemical Kinetics*, Vol. 31, No. 2, 1999, pp. 113–125.

[53] Schwer, D. A., Corrigan, A. T., and Kailasanath, K., "Towards efficient, unsteady, three-dimensional rotating detonation engine simulations," *52nd Aerospace Sciences Meeting*, 2014, p. 1014.